A&A 453, 979–987 (2006)
DOI: 10.1051/0004-6361:20053741

Astronomy & Astrophysics

Odin⋆ CO and ^{13}CO $J = 5$–4 mapping of Orion KL – a step towards accurate water abundances

E. S. Wirström[1], P. Bergman[1,2], A. O. H. Olofsson[1], U. Frisk[3], Å. Hjalmarson[1], M. Olberg[1], C. M. Persson[1], and Aa. Sandqvist[4]

[1] Onsala Space Observatory, Chalmers University of Technology, 43992 Onsala, Sweden
e-mail: eva@oso.chalmers.se
[2] European Southern Observatory, Alonso de Cordova 3107, Vitacura, Casilla 19001, Santiago, Chile
[3] Swedish Space Corporation, PO Box 4207, 17104 Solna, Sweden
[4] Stockholm Observatory, SCFAB-AlbaNova, 10691 Stockholm, Sweden

Received 1 July 2005 / Accepted 23 March 2006

ABSTRACT

Aims. The very high main beam efficiency (90%) of the telescope on the sub-millimetre wave satellite Odin, in combination with the small calibration errors in the absence of atmospheric attenuation, assures that observed line brightness temperatures are very accurately determined. Based on this, we attempt to determine the column density distribution of H_2, and the ortho-water abundance, in the Orion KL region.

Methods. We have, for the first time, mapped the ^{12}CO $J = 5$–4 emission in a $7' \times 7'$ region covering Orion KL, observed simultaneously with a ^{13}CO $J = 5$–4 map. Also presented are C^{18}O $J = 5$–4 emission data at four different positions and a C^{17}O $J = 5$–4 emission spectrum detected towards the Orion KL position. The Odin mapping was performed at $1'$ spacing (beam full width at half maximum $126''$ at 557 GHz).

Results. The CO $J = 5$–4 narrow line emission from this region mainly arises in the warm, dense gas at the interface (the photon-dominated region) between the M 42 H II region and the Orion A molecular cloud, the Orion PDR. The ^{12}CO and ^{13}CO $J = 5$–4 emission maps have been used to determine the column density distribution of H_2 gas across the Orion KL region. The results have been verified by comparing to column densities obtained using the decidedly optically thin C^{18}O emission as input to the RADEX radiative transfer code. We find H_2 column densities ranging from 5×10^{21} cm^{-2} at map edges to 7×10^{22} cm^{-2} at the molecular ridge. The mass of the gas in the mapped region is estimated to be 480 $M_\odot$, of which 320 $M_\odot$ is situated towards the molecular ridge. We estimate that about half of this mass belongs to the warm Orion PDR interface layer. Finally, based on data from the positions where C^{18}O $J = 5$–4 has been observed, we estimate the ortho-water abundance in the Orion PDR layer to be $\geq 8 \times 10^{-8}$, higher than previously estimated.

Key words. ISM: individual objects: Orion KL – ISM: molecules – radio lines: ISM, HII regions – submillimeter

1. Introduction

Situated at a distance of only 500 pc, the Orion KL region is one of the prime targets for studying massive star formation and its interaction with the environment. Extensive observational investigations in the mm and sub-mm range (see Genzel & Stutzki 1989, for a review) have revealed that the morphology of the molecular gas is largely dominated by the M 42 H II region, situated in front of the Orion A molecular cloud, and the high velocity outflows of the mid-infrared (IR) Orion KL nebula.

The pioneering work by Schmid-Burgk et al. (1989) and Graf et al. (1990) showed that the mid-J (6–5, 7–6) CO and ^{13}CO emission from the Orion KL region mainly originates in warm (∼100 K), dense (∼10^5 cm^{-3}) and quiescent ($\Delta v \approx 5$ km s^{-1}) gas. The observed high temperatures, combined with relatively low velocities, excluded scenarios where shocks or collisions are responsible for the heating of the gas, leaving the non-ionising ultraviolet (UV) radiation from the Trapezium OB stars as the most plausible explanation.

The UV field of the Trapezium stars has ionised the surrounding gas, creating the M 42 H II region. At all the interfaces between ionised and molecular gas the temperature and chemistry are dominated by the non-ionising UV photons in a photon-dominated region (PDR), but the main gas component is molecular hydrogen and the density is high enough for simple molecules and radicals to be present in detectable columns. The M 42 H II region is about $5'$ in diameter (Zuckerman 1973; Yusef-Zadeh 1990), so a large part of the molecular gas in the Orion KL region has a layer of warm PDR gas facing us. We will refer to this interface as the Orion PDR, and it is only in the direction of this region where the *SWAS* and Odin satellites have observed uniquely strong and extended narrow-line ortho-H_2O (1_{10}–1_{01}) emission (Snell et al. 2000; Olofsson et al. 2003; Melnick & Bergin 2005). Since water plays an important role both as an oxygen reservoir and as a coolant in molecular clouds, it is very interesting, if possible, to measure its abundance across this region. This may be achieved using the ortho-H_2O water maps mentioned above, if the H_2 column density of the same gas can be determined as accurately as possible.

The general structure of the Orion PDR gas has been mapped in the high-density tracer CN (Rodríguez-Franco et al. 1998;

⋆ Odin is a Swedish-led satellite project funded jointly by the Swedish National Space Board (SNSB), the Canadian Space Agency (CSA), the National Technology Agency of Finland (Tekes), and the Centre National d'Études Spatiales (CNES, France). The Swedish Space Corporation (SSC) was the industrial prime contractor and is also responsible for the satellite operation.

Rodríguez-Franco et al. 2001), outlining the S-N oriented molecular ridge, the Orion Bar, the Northern bars, as well as gas at the far side of the H II region. Together, these gas condensations constitute the boundaries of the M 42 H II region. The original notion that the mid-J CO narrow-line emission arises in the Orion PDR has been further supported by its similarity in both intensity distribution and line profiles to forbidden [C II] and [O I] fine-structure lines (Stacey et al. 1993; Herrmann et al. 1997).

Towards the KL position CO emission is detected over a much wider velocity range (first noted over >150 km s^{-1} in CO $J = 1-0$ by Zuckerman et al. 1976). The VLBI proper motion observations of H_2O masers by Genzel et al. (1981) showed that the high-velocity gas emission originates in two separate, almost perpendicular flows. The same outflow morphology was also found for the CO gas in interferometer maps by Masson et al. (1987) and for SiO (Wright et al. 1995; Plambeck et al. 2003). The high-velocity flow emission has a full width at zero power (FWZP) of up to 200 km s^{-1} and is bipolar in nature, extending in the SE-NW direction over a $>30 \times 20''$ area (Masson et al. 1987). The low-velocity flow emission has been suggested to originate in an expanding disk-like structure, elongated in the SW-NE direction. It has a FWZP of about 35 km s^{-1} (the "18 km s^{-1} flow") and a spatial extension of $>20 \times 10''$ (Masson et al. 1987). The shocks that inevitably are created when the high velocity flow plunges into the surrounding medium have been studied in emission from highly rotationally excited CO and vibrationally excited H_2 (Watson et al. 1985; Salas et al. 1999; Gustafsson et al. 2003; Kristensen et al. 2003).

Using the sub-millimetre satellite Odin we have, for the first time, mapped the ^{12}CO $J = 5-4$ emission in the Orion KL region, simultaneously with ^{13}CO $J = 5-4$. Large-scale mapping of the Orion molecular cloud in this transition of ^{13}CO has previously been done by *SWAS* (Plume et al. 2000) with approximately twice the Odin beam size. The $J = 5-4$ rotational transitions of CO and ^{13}CO should trace the warm gas of the Orion PDR since their upper state energies are 83 and 79 K, respectively. The critical density of this CO transition is $\sim 5 \times 10^4$ cm^{-3} so this emission is easily thermalised in the dense PDR gas. The high data quality and spectral resolution, paired with the very high main beam efficiency of the Odin telescope (90%), and the absence of any atmospheric absorption uncertainties, have allowed us to analyse the distribution and kinematics of the gas in the Orion KL region. Together with simultaneous ortho-H_2O maps (see e.g. Olofsson et al. 2003) these data will make it possible to determine the H_2O abundance variations in the Orion PDR. In this paper, we provide estimates of the H_2O abundances in three positions where the C^{18}O, ^{13}CO and CO $J = 5-4$ lines have been observed by Odin.

2. Observations

The CO and ^{13}CO $J = 5-4$ lines were observed simultaneously with the Odin sub-millimetre wave spectroscopy satellite over a $7' \times 7'$ area. The data discussed here were acquired at three occasions in 2004, during nine orbits each, March 15 to 16, April 13 to 14 and August 27 to 28, resulting in 1–3 min on-source integration time per position. The single side-band (SSB) system temperature was $T_{\rm sys} = 3500$ K.

Different spectrometers were used for the two lines. The CO spectra were taken with the acousto-optical spectrograph (AOS, 0.62 MHz channel spacing, ~1050 MHz bandwidth centred at 576.268 GHz) while the ^{13}CO data were taken with the hybrid autocorrelator spectrometer (AC, 0.50 MHz channel spacing, ~420 MHz bandwidth centred at 550.926 GHz), see Olberg et al. (2003).

The sky switching mode, with reference sky beams at 42° distance and 4.4° *FWHM*, was used for recording the data, and the chopper wheel method was used for calibration (Frisk et al. 2003; Olberg et al. 2003). The maps were acquired as an observing grid consisting of 8×8 grid-points separated by 60″, i.e., about half the beam width (beam *FWHM* 126″ at 557 GHz, Frisk et al. 2003), in both right ascension (RA or α) and declination (Dec or δ). The (0′, 0′) map position is at the Orion KL coordinates $\alpha = 5^{\rm h}35^{\rm m}14\overset{\rm s}{.}36$, $\delta = -5°22'29\overset{''}{.}6$ (J2000). The telescope pointing was checked simultaneously with these observations by mapping of the Orion KL water outflow and the pointing offset, including attitude reconstruction, was found to be less than 15″. The calibration uncertainty was estimated using the variation of the ^{13}CO integrated intensity of spectra from six different mapping occasions during 2003 and 2004. It was found to be less than 10%. All intensities in this paper are given in units of antenna temperature, $T_{\rm A}$. The telescope main beam efficiency, $\eta_{\rm mb} = 0.9$ (Frisk et al. 2003), is taken into account in the column density estimates.

In addition we have used Odin to observe the C^{18}O $J = 5-4$ line in four chemically interesting positions from Ungerechts et al. (1997) [(0′, 0′), (0′, −2′) at the Southern dense core and outflow, (+2′, −2′) at the Orion Bar, and (+1′, +3′) at the "radical-ion peak", all with respect to the Orion KL position, see Fig. 1]. The data discussed here were acquired during 29 orbits at the end of March 2003 ($T_{\rm sys} = 3600$ K) resulting in 2–3 h of integration time per position. The AOS spectrometer was used as back-end. We also present a spectrum of C^{17}O $J = 5-4$ in the (0′, 0′) position, observed during the Orion spectral scan campaign (Olofsson et al., in prep.).

3. Results

Figure 1 displays the integrated intensity distribution of the position-averaged ^{13}CO $J = 5-4$ emission. That is, in each position a number of 5 second-spectra have been averaged using the integration time divided by $T_{\rm sys}^2$ as weight. The map clearly shows that the ^{13}CO emission mainly originates in the dircetion of the extended molecular ridge and is not particularly dominated by outflow emission from Orion KL at (0′, 0′). ^{13}CO is detected in all map positions. At the offset position (−3′, +4′), where ^{13}CO is weakest, the peak intensity is 2 K and this is well above a 5σ detection.

The antenna temperature distribution of the position-averaged ^{12}CO $J = 5-4$ map, taken at the same occasion, is presented in Fig. 2, showing that the ^{12}CO line temperatures range from 40–80 K across the molecular ridge. Since the 50 to 100 μm colour temperature of the dust at the PDR of the Orion Bar is ~70 K at 1′ resolution (Werner et al. 1976), indirect heating by non-ionising UV photons must be important in the gas we observe (as also deduced by Graf et al. 1990). This is typically the case near the surface of a PDR where the dust is readily cooled by far-infrared (FIR) continuum radiation, but the gas mainly cools via much less efficient [C II] and [O I] line emission (Hollenbach & Tielens 1997). Thus, the high ^{12}CO line temperatures confirms that this emission mainly traces the warm molecular gas of the Orion PDR. The origin of the ^{13}CO $J = 5-4$ emission along the line-of-sight is less clear and is discussed further in Sect. 4.3.

The maps showing all ^{12}CO and ^{13}CO spectra are presented in Fig. 3. Overall, line peak velocities from Gaussian fits,

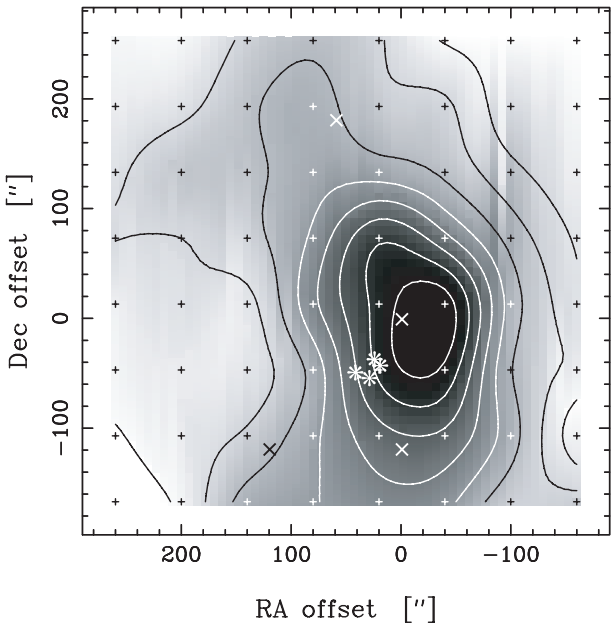

Fig. 1. The Odin ^{13}CO J = 5−4 integrated intensity map from August 2004. Contours mark every 20 K km s^{-1} from 20 K km s^{-1} to 160 K km s^{-1}. Map positions (marked with "+") are shifted by (+20″, +13″) relative to (0″, 0″) according to the attitude reconstruction. Positions where C^{18}O has been observed are marked with "×" and the four brightest Trapezium star positions with 8-pointed stars.

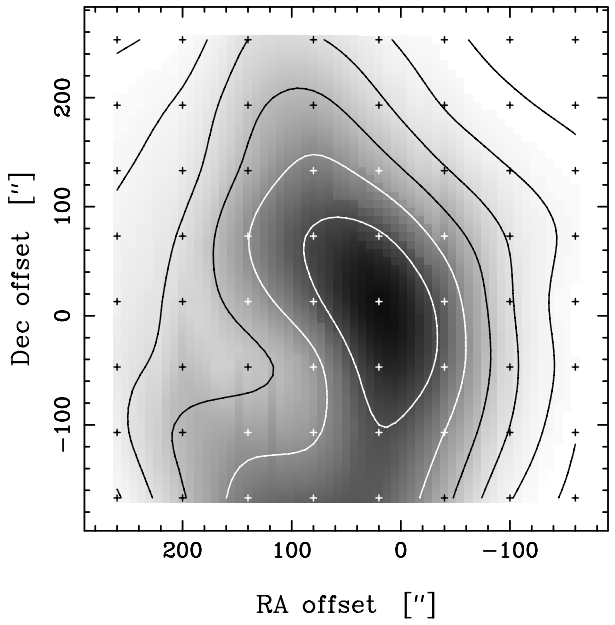

Fig. 2. The Odin CO J = 5−4 antenna peak temperature map from August 2004. Contours mark every 10 K from 20 K to 70 K. Map position offsets are marked with "+" and are the same as in Fig. 1.

varying from 8 to 10 km s^{-1}, agree well with the recently published J = 9−8 data (Marrone et al. 2004). We have also convolved our ^{13}CO map to a resolution corresponding to that of the ^{13}CO J = 5−4 *SWAS* observations (Plume et al. 2000) and compared lines in several positions. The close similarity in intensities (better than 10%) and line profiles demonstrates consistency in both velocity and amplitude calibration of the two telescopes.

Figure 4 compares our spectra of ^{12}CO, ^{13}CO and C^{18}O J = 5−4 with the H_2O (1_{10}−1_{01}) spectra from Olofsson et al. (2003) in the positions where C^{18}O has been observed (except KL). The line-shapes are similar within each position, even though the water lines have a somewhat more triangular form. Note also that the signal-to-noise ratio in the water emission spectra is less than half that of the CO spectra.

As is evident in Fig. 4, there is a systematic velocity shift between ^{13}CO and C^{18}O emission peaks in all three positions. Likewise, there appears to be a shift between ^{13}CO and ^{12}CO in one position. We can presently not ascribe this effect to instrument errors, since measurements have been frequency calibrated by observing strong emission lines in the Earth's atmosphere on several occasions, giving consistent results. If indeed real, the shifts could be due to the varying line opacities in the CO isotopologues. However, proving such effects would require detailed radiative transfer and source morphology modelling, which is beyond the scope of this Paper.

At the KL position the four CO isotopologues; ^{12}CO, ^{13}CO, C^{18}O and C^{17}O, have been observed (Fig. 5). Here the typical outflow line profiles with extended line wings are prominent in ^{12}CO with a FWZP of 120 km s^{-1}. If we correct for the Odin 126″ beam-size, the high-velocity outflow is present across a 100″ area around the (0′, 0′) map position, but not with as large velocity range. This is consistent with high-velocity CO J = 7−6 emission which is detected across a ∼100″ area by Wilson et al. (2001). In ^{13}CO, and even C^{18}O and C^{17}O, weaker line wings are present in the KL position. As can also be seen in Fig. 5, the ^{12}CO J = 5−4 outflow has excess emission in the blue wing over the red wing (by 25% as measured in the velocity range 10−40 km s^{-1} from the line centre at 9 km s^{-1}). The same type of asymmetry has been reported for the J = 4−3 line by Wilson et al. (2001) and for the J = 7−6 line by Howe et al. (1993).

4. Analysis and discussion

4.1. Velocity structure

The extended line wings and the narrow central peak of the ^{12}CO J = 5−4 emission line in the KL position suggest that the following three velocity structures are present in the Odin antenna beam: emission from the low- and high-velocity outflows of KL, and the warm, dense layer of the Orion PDR. Emission from the hot core region, at about 5 km s^{-1}, cannot be distinguished in the line profiles since the emission from the cloud surface is optically thick. Moreover, the size of the hot core (∼10″) makes it very diluted in the large Odin beam. Assuming that towards the KL position the three structures do not overlap each other spatially, and have approximately Gaussian velocity distributions, we may analyse them separately by a least-squares fit of Gaussians to the line profiles. The ^{13}CO J = 5−4 emission line does not contain any emission above the noise level at velocities higher than 20 km s^{-1} from line centre, so in this case we have to fit two Gaussians, representing the narrow emission and the low-velocity flow respectively. Since high-velocity flow emission is absent in this line, the risk for "contamination" in the fitted low-velocity flow component is low. In order to avoid such contamination as far as possible in the three component fit to the ^{12}CO J = 5−4 emission line, we fix the velocity width of the low-velocity component to that obtained for the ^{13}CO line and adjust the other parameters to a best least-squares fit. The results are presented in Fig. 6 and Table 1.

In the eastern part of the map, at RA offsets +140″ to +260″, two velocity components, at 6 and 10 km s^{-1}, are clearly seen in both the ^{13}CO and ^{12}CO emission (Fig. 3). The same two

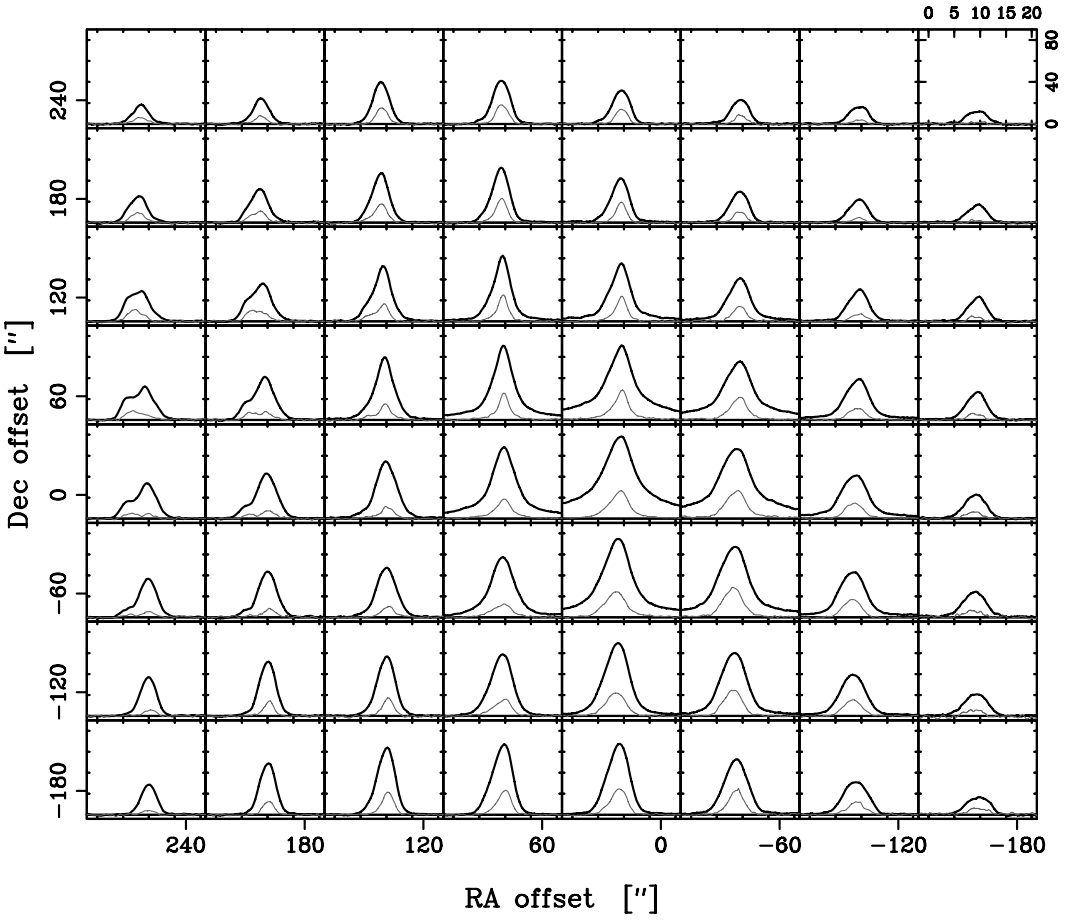

Fig. 3. The Odin CO (black) and ^{13}CO (grey) J = 5−4 position-averaged emission line maps from August 2004. The velocity and intensity scales are given, in units of km s^{-1} and K respectively, next to the top right spectrum. To visualise the velocity structure of the spectral lines we here only show a limited velocity range from about 0 to 20 km s^{-1}. Map positions are shifted by (+20″, +13″) relative to (0″, 0″) according to the attitude reconstruction.

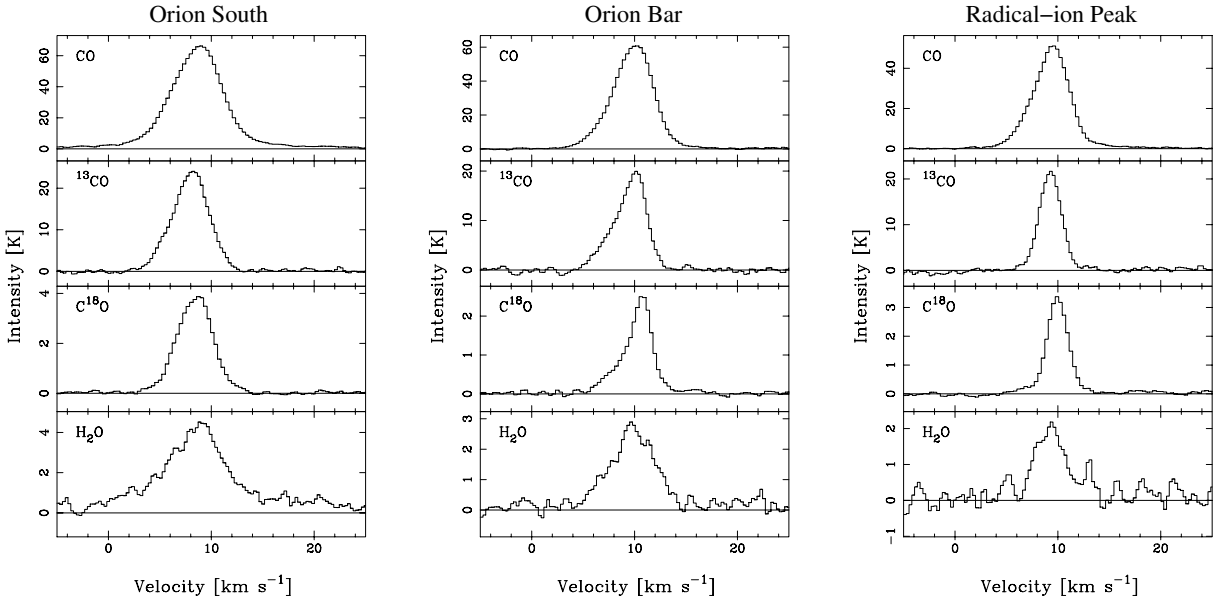

Fig. 4. Spectra of the three most abundant isotopologues of CO J = 5−4 together with H_2O (1_{10}−1_{01} at 557 GHz, from Olofsson et al. 2003) in the three positions; the Southern dense core (0, −2′); the Orion bar (+2′, −2′); and the Radical-ion peak (+1′, +3′).

components have also been observed with a 20″ antenna beam in ^{13}CO J = 2−1 by Greaves & Church (1996); thus the two velocity components coincide also at small spatial scales. We believe that the 6 km s^{-1} component originates in the so-called Northern, or North-Eastern, bar. This is an elongated, molecular structure that seems to confine the H II region of the Trapezium

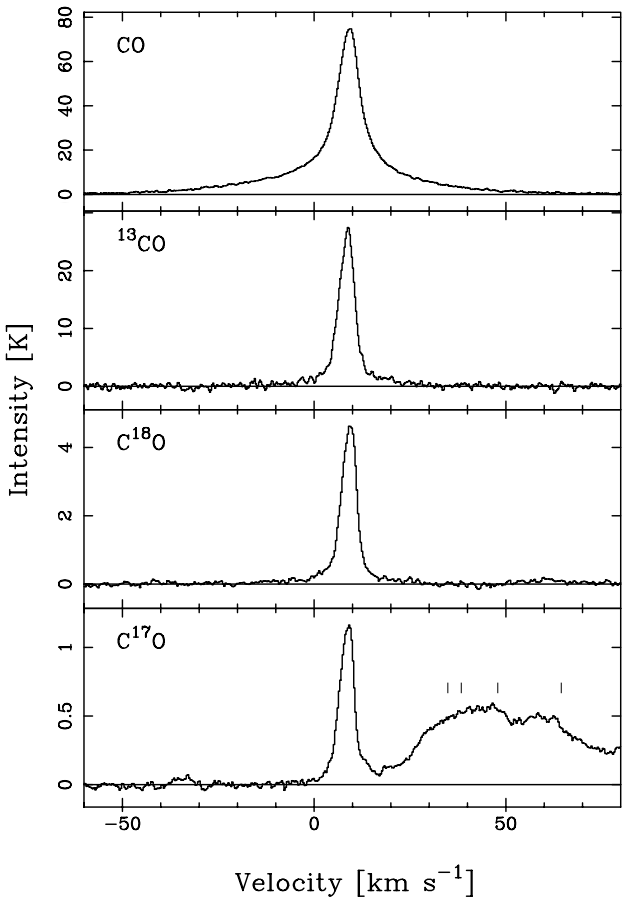

Fig. 5. CO, ^{13}CO, C^{18}O and C^{17}O J = 5−4 lines towards Orion KL. Four SO_2 lines, with typical wide outflow line-shapes, are marked in the C^{17}O spectrum. Note the different vertical scales.

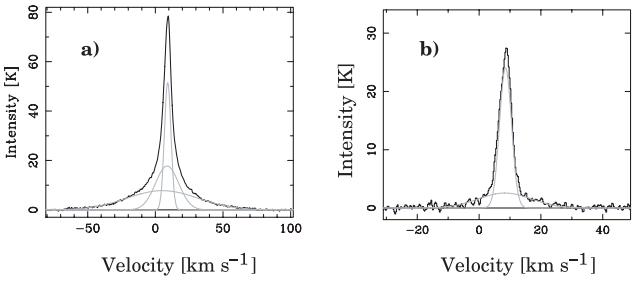

Fig. 6. The ^{12}CO (a) and ^{13}CO (b) spectra from the KL position (in black) with the Gaussians (in grey) that makes the best fit to the respecitve spectral line shape. The Gaussian parameters are presented in Table 1.

Table 1. Gaussian parameters for the least-squares fits of the ^{12}CO and ^{13}CO emission at the Orion KL position. The width of the ^{12}CO low-velocity flow component was fixed to 20.2 km s^{-1}, as obtained from the ^{13}CO fit. Errors are only due to noise, no calibration errors included.

Component	Isotope	v [km s^{-1}]	Δv [km s^{-1}]	Ampl. [K]
Narrow	^{12}CO	9.1 ± 0.1	5.7 ± 0.1	51.5 ± 0.2
Narrow	^{13}CO	8.6 ± 0.3	4.5 ± 0.1	24.0 ± 0.2
Low-vel. flow	^{12}CO	8.7 ± 0.1	20.2	17.7 ± 0.2
Low-vel. flow	^{13}CO	8.3 ± 0.3	20.2 ± 0.8	2.6 ± 0.2
High-vel. flow	^{12}CO	5.2 ± 0.2	62.0 ± 0.4	7.8 ± 0.1

cluster to the North, similar to the Orion Bar in the south, but not as strong in emission and being more fragmented/clumpy. The North-Eastern bar has been observed in many molecules and the emission shows velocities 5−10 km s^{-1} (e.g. Greaves & Church 1996; Fuente et al. 1996; Rodríguez-Franco et al. 1998). The J = 5−4 intensities observed in Odin's 126″ antenna beam at the North-Eastern bar, at offset (+260″, +133″), are $T_{\rm mb}$(^{12}CO) = 32 K and $T_{\rm mb}$(^{13}CO) = 12 K, while Greaves & Church (1996) report a ^{13}CO J = 2−1 main beam brightness temperature of 31 K at their North-Eastern bar peak at offset (+257″, +113″), in a beam size of ∼20″. A large column of colder (T < 50 K) gas could give rise to the observed absolute and relative brightness temperatures, but it is more likely that the J = 2−1 emission mainly arises in cooler gas, possibly in denser clumps, while the bulk of the J = 5−4 line is emitted from warm (inter-clump) gas.

4.2. Temperatures

In the column density analysis below we have adopted kinetic temperatures of the molecular gas equal to the ^{12}CO J = 5−4 peak main beam brightness temperature. Theoretically this is an adequate lower limit and in comparable positions (2′S and the Bar) these temperatures are about 40% lower than those derived from LVG analysis of several CO transitions by Marrone et al. (2004). The large main beam efficiency of Odin guarantees that not much of the extended emission is added to the intensity through the side-lobes. This can otherwise be a problem for observations at these high frequencies; the beam size of a ground-based telescope is often very small, but the main beam efficiency then goes below 0.5 which gives rise to large error bars.

Since the noise level is too high in our ^{13}CO spectrum toward Orion KL we cannot decide whether the CO J = 5−4 high velocity outflow emission is optically thick or thin. In addition, neither of the outflows are spatially resolved in the Odin beam. Maps of nearby CO transitions show spatial maximum half power extensions of the low- and high-velocity flows ≤60″ (J = 7−6 Wilson et al. 2001; J = 4−3 Schulz et al. 1995). This is consistent with the interferometric observations of CO J = 1−0 by Masson et al. (1987), which were insensitive to structures >30″ and showed spatial extensions of 20 × 10″ and 30 × 20″ for the low- and high-velocity flow, respectively. Observations of the low- and high-velocity outflows, as traced in H_2O masers by Genzel et al. (1981) also indicate outflow sizes within this limit. To be conservative when we correct the ^{12}CO J = 5−4 emission for the apparent beam dilution, we thus assume intrinsic Gaussian source profiles with *FWHM* 60″. We then get brightness temperatures of 106 ± 11 K and 47 ± 5 K (including 10% calibration errors) from the Gaussian line profile fits of the low- and high-velocity flows, respectively. We verify these outflow peak brightness temperatures by noticing that their sum (∼150 K) is lower than the peak CO J = 4−3 and J = 7−6 $T_{\rm mb}$ (∼200 K) towards the same position as presented by Wilson et al. (2001). The kinetic temperatures of the two outflows have to be higher than their respective peak brightness temperatures, but are otherwise hard to estimate from our data. Instead we have adopted a kinetic temperature of 150 K for the low-velocity flow, according to a lower limit derived from HDO and water observations (Pardo et al. 2001), and 100 K for the high-velocity flow, somewhat lower than excitation temperatures of the very wide SO_2 lines according to several studies (e.g. Schilke et al. 2001; Schloerb et al. 1983).

Table 2. Integrated intensities and isotopic ratios. Given integrated intensity uncertainties are only due to noise while a calibration error of 10% is included in the ratio uncertainties.

Position rel. to KL	$I(^{12}CO)$ [K km s^{-1}]	$I(^{13}CO)$ [K km s^{-1}]	$I(C^{18}O)$ [K km s^{-1}]	$I(C^{17}O)$ [K km s^{-1}]	$\frac{I(^{12}CO)}{I(^{13}CO)}$	$\frac{I(^{13}CO)}{I(C^{18}O)}$	$\frac{I(C^{18}O)}{I(C^{17}O)}$
(0′, 0′) Narrow	311 ± 5	114 ± 3	26.8 ± 0.2	6.2 ± 0.1	2.7 ± 0.6	4.3 ± 0.9	4.3 ± 0.6
(0′, 0′) Low vel. flow	379 ± 4	56 ± 4	–	–	6.8 ± 1.5	–	–
(0′, 0′) High vel. flow	513 ± 7	–	–	–	–	–	–
(0′, −2′)[a]	446 ± 1	106 ± 1	17.8 ± 0.2	–	4.2 ± 0.6	6.0 ± 0.9	–
(+2′, −2′)[b]	302 ± 1	73 ± 1	8.8 ± 0.2	–	4.1 ± 0.6	8.3 ± 1.2	–
(+1′, +3′)[c]	231 ± 1	59 ± 1	9.3 ± 0.2	–	3.9 ± 0.6	6.3 ± 0.9	–
(−3′, +4′)[d]	55 ± 1	4.4 ± 0.6	–	–	12.5 ± 2.4	–	–
(+4′, +2′)[e]	176 ± 1	45 ± 1	–	–	3.9 ± 0.6	–	–

[a] Southern dense core position. [b] Orion Bar position. [c] "Radical-ion peak" position. [d] Position of lowest intensity. [e] North-Eastern Bar position.

4.3. Column densities

Integrated intensity ratios in various map positions can provide information of the optical depths of the isotopic lines. For this purpose we have adopted constant isotopic abundance ratios of $[CO]/[H_2] = 8 \times 10^{-5}$, $[CO]/[^{13}CO] = 60$, $[CO]/[C^{18}O] = 490$ (e.g. Wilson & Matteucci 1992), which gives $[^{13}CO]/[C^{18}O] = 8.2$, and $[C^{18}O]/[C^{17}O] = 4$ (e.g. Bensch et al. 2001). Table 2 presents the resulting integrated intensity ratios in some positions and structures of interest. Judging from the observed ^{12}CO to ^{13}CO ratio the ^{12}CO $J = 5{-}4$ emission is optically thick across the mapped region ($\tau > 5$), including the position of weakest intensity (Table 2), while the ^{13}CO $J = 5{-}4$ emission is not far from being optically thin ($\tau_{13} \lesssim 0.6$). The largest τ_{13} is found in the (0′, 0′) position where the I_{12}/I_{13} ratio is as low as 2.7 (Table 2). From the already low optical depth of the ^{13}CO $J = 5{-}4$ emission we also conclude that the emission from the same transition in the less abundant isotopologues, $C^{18}O$ and $C^{17}O$, is optically thin at all positions where it has been observed, e.g. at (0′, 0′) where $\tau_{18} \sim 0.2$ (Table 2).

From its high optical depth and peak temperatures, we may conclude that the ^{12}CO $J = 5{-}4$ emission provides a measure of the excitation temperature of the warm Orion PDR gas. This is in line with the difference found between the temperature tracers ^{12}CO $J = 1{-}0$ and CH_3C_2H $J = 6{-}5$ in Orion by Bergin et al. (1994), where even the ground state CO transition was found to trace warm surface gas, while the temperature within the ridge was found to be about 40 K from the optically thin CH_3C_2H. The excitation temperatures from ^{12}CO $J = 5{-}4$ can be used in a simple LTE analysis, together with the (almost) optically thin ^{13}CO emission, to estimate the CO (and hence H_2) column density distribution across this region.

However, since the ^{13}CO $J = 5{-}4$ emission is close to optically thin, it should have its origin both in the warm Orion PDR gas and in the colder molecular ridge gas behind, traced by e.g. CH_3C_2H and ^{13}CO $J = 1{-}0$. In order to estimate how large the respective fractions are, we assume that the physical conditions in the two components are the same ($n(H_2) = 10^5$ cm^{-3}, $\Delta v = 5$ km s^{-1}), except for the kinetic temperature which is approximately 40 K in the ridge and 80 K in the PDR. From the $J = 1{-}0$ and $2{-}1$ ^{13}CO analysis by Castets et al. (1990) we get an estimate of the ^{13}CO column density of the ridge component. Castets et al. find values just below 5×10^{16} cm^{-2} in our region of interest. From a RADEX on-line analysis (see below) we can then directly see that this column density only can account for no more than 40% of the observed ^{13}CO $J = 5{-}4$ emission. Furthermore, to explain the remaining 60% of the emission we need a ^{13}CO PDR column density of at least the same size (i.e. 5×10^{16} cm^{-2}). The CO (and hence H_2) column density distribution of warm, foreground PDR gas can thus be estimated from the combination of ^{13}CO emission and excitation temperature from ^{12}CO. The decidedly optically thin $C^{18}O$ emission traces approximately the same gas as ^{13}CO.

The molecular gas distribution in the Orion region shows signs of clumping on different scales, most studied at the PDR of the Orion Bar. Here high density clumps of $n(H_2) \gtrsim 10^6$ cm^{-3} are embedded in a less dense inter-clump medium with $n(H_2) = 10^4{-}10^5$ cm^{-3} (Young Owl et al. 2000). Lis & Schilke (2003) have shown that the mid-J CO emission from this specific region most likely originates in the warmer and more evenly distributed inter-clump medium. Since our $7' \times 7'$ maps are dominated by the Orion PDR, we adopt an H_2 density of 10^5 cm^{-3}for the bulk of the CO $J = 5{-}4$ emitting gas in our analysis, corresponding to the warm, inter-clump PDR gas. The outflow has been shown to be somewhat denser so we assume $n(H_2) = 10^6$ cm^{-3} (e.g. Schulz et al. 1995) for both the high and low velocity part. We note that the $J = 5{-}4$ excitation temperatures, and hence the column densities, from radiative transport models are not very sensitive to variations in the gas density if it is above 5×10^4 cm^{-3}, since this is approximately where the CO $J = 5{-}4$ emission becomes thermalised.

Observed line intensities and widths (*FWHM*) for the optically thin lines of $C^{18}O$, $C^{17}O$ and, at the bar position also ^{13}CO, have been used, together with the temperature and density assumptions previously discussed, as input to the RADEX[1] radiative transfer code (Schöier et al. 2005) to estimate the beam-averaged CO column densities. The results, shown in Table 3, have been validated by comparing to the observed ^{13}CO to $C^{18}O$ integrated intensity ratios in the non-outflow cases. However, for the low-velocity outflow, the ^{12}CO to ^{13}CO ratio is probably misleading and does not match the column densities obtained with RADEX. The likely reason is that the imposed Gaussian line shape will underestimate the ^{12}CO integrated emission of the low-velocity flow, since this expanding disk-like structure actually has a rather rectangular line shape (Genzel et al. 1981; Wright et al. 1995; Plambeck et al. 2003), and too much emission is attributed to the high-velocity flow. However, this does not affect the ^{13}CO outflow fit.

The momentum and kinetic energy of the outflows have been estimated from summing over 1 km s^{-1} velocity intervals of fitted Gaussian line profiles (i.e., $p = \sum m_v v$ and $E_{\rm kin} = \frac{1}{2} \sum m_v v^2$). This method does not take into account inclination effects (intrinsic velocities may be higher than the observed radial velocities), which means the results can be interpreted as lower

[1] http://www.strw.leidenuniv.nl/~moldata/radex.php

Table 3. Beam-averaged column densities obtained through RADEX on-line, and ortho-water abundance estimates (see Sect. 4.4).

Position rel. to KL	$n(H_2)$ [cm^{-3}]	T_{kin} [K]	Isotope used	Δv [km s^{-1}]	N(CO) [10^{18} cm^{-2}]	N(CO)[a] [10^{18} cm^{-2}]	x(o-H_2O) [10^{-8}]
(0′, 0′) Narrow	10^5	83	$C^{17}O$	5.0	5.4 ± 1.2	4	
(0′, 0′) Narrow	10^5	83	$C^{18}O$	5.0	5.6 ± 0.6		
(0′, 0′) Low vel. flow	10^6	150	^{13}CO	20	1.8 ± 0.3 9.8 ± 1.4[e]		
(0′, 0′) High vel. flow	10^6	100	^{12}CO	62	0.3 ± 0.1 1.8 ± 0.3[e]		
(0′, −2′)[b]	10^5	74	$C^{18}O$	4.1	4.0 ± 0.4	3	10.6[f]
(+2′, −2′)[c]	10^5	68	$C^{18}O$	3.0	2.0 ± 0.2	1.5	9.4[f]
(+2′, −2′)[c]	10^5	68	^{13}CO	3.6	3.1 ± 0.5		
(+1′, +3′)[d]	10^5	57	$C^{18}O$	2.4	2.5 ± 0.3	1.7	4.0[f]

[a] Simple LTE model results, assuming optically thin ^{13}CO emission. [b] Southern dense core position. [c] Orion Bar position. [d] "Radical-ion peak" position. [e] Assuming a source size of 60″. [f] Using 50% of the reference CO column (see Sect. 4.3).

limits. The LVG method was used on the ^{13}CO (low-velocity) and the ^{12}CO (high-velocity) Gaussian fits (Table 1) to calculate the column density, and implied H_2 mass, in each interval. The total column density of each flow resulting from this method is consistent with that obtained by RADEX (Table 3). The low-velocity flow has a total momentum of 180 $M_\odot$ km s^{-1}, and a total kinetic energy of 1.9×10^{46} erg, to which the blue wing ($v < 9$ km s^{-1}) contributes 56%. The total high-velocity flow has $p = 90$ $M_\odot$ km s^{-1} and $E_{kin} = 3.0 \times 10^{46}$ erg, to which the blue wing ($v < 9$ km s^{-1}) contributes 60%. The total outflow energy, of low- and high-velocity flow combined, falls within the limits calculated from ^{12}CO and ^{13}CO $J = 2-1$ and $J = 1-0$ by Margulis & Lada (1985), but the total momentum is somewhat higher (∼10%) than their upper limit. The reason for the agreement in one case but not the other, is that our Gaussian shapes include low-velocity gas, while Margulis & Lada only take the line-wings into account. This difference in method gives us almost an order of magnitude higher total molecular flow mass, which, in case of the kinetic energy, becomes less important because of the v^2 term in the energy product. We believe that the main reason why our new results show lower limits at least 50% above the previous ones, is the too low excitation temperature assumed by Margulis & Lada (1985).

Our estimated H_2 column density of the low-velocity flow, 1.2×10^{23} cm^{-2}, for a 60″ size source size and not averaging over the large Odin beam, is consistent with the range derived by Masson et al. (1987), $(3-10) \times 10^{22}$ cm^{-2}. Not many column density estimates have been produced for the high-velocity flow separately, but in the Orion review by Genzel & Stutzki (1989) a value of 5×10^{22} cm^{-2} was presented for H_2. The column density we have derived, assuming a Gaussian line shape, (see Table 3) is in reasonable agreement with this.

In the Orion Bar position the column density derived from ^{13}CO is about 50% higher than that derived from $C^{18}O$. This discrepancy can be accounted for if the abundance ratio at this position is $[^{13}CO]/[C^{18}O] = 10$, only slightly higher than 8.2 as assumed for the rest of the map. This also provides better agreement with the observed ^{13}CO to $C^{18}O$ intensity ratio. Similarly high abundance ratios $[^{13}CO]/[C^{18}O]$ were observed towards the Orion bar by White & Sandell (1995) in the $J = 2-1$ transition. They explain this phenomenon in terms of chemical fractionation on clump surfaces in the PDR.

The other beam-averaged column densities calculated using RADEX agree well with what has previously been found from ro-vibrational lines of CO near KL (González-Alfonso et al. 2002), $C^{18}O$ $J = 2-1$ from the high density cores at KL and 2′ S (Wilson et al. 1999), a CO multi-transition study including 2′ S (Marrone et al. 2004), and ^{12}CO $J = 6-5$ observations of the KL outflow (Koepf et al. 1982). The average column density on large scales (∼20′ × 40′), from the ^{13}CO $J = 5-4$ *SWAS* mapping using LVG analysis (Plume et al. 2000), is lower than our results, but then our observations only cover the region of most intense emission where their column density has its peak.

Also presented in Table 3 are column densities calculated by the simplified LTE analysis described above, assuming optically thin ^{13}CO. In general we see that this method underestimates the column densities by 25% compared to RADEX results from $C^{18}O$ input. The main source of the discrepancy is the lack of optical depth correction, while the method is very insensitive to variations of the excitation temperature in the range 50−140 K. We therefore use this method to get a rather reliable estimate of the H_2 column density distribution over the whole region (see Fig. 7). The largest H_2 columns are found along the ridge and at the North-Eastern bar. The map shows only a hint of the Southern bar while the column is clearly decreasing at the Dark Bay area. This column density distribution is similar to the intensity distributions of CO $J = 7-6$ (Schmid-Burgk et al. 1989), [C II] and [O I] (Stacey et al. 1993; Herrmann et al. 1997), except for the Northern bar column density enhancement which is shifted 2′ to the north as compared to the atomic emission. Our column density increase coincides better with one of the dense gas Northern bars seen in CN ($N = 1-0$) and CN ($N = 2-1$) (Rodríguez-Franco et al. 1998). The column density features discussed are even more pronounced in our first attempts to deconvolve the maps to 40″ beam size. Here we have applied a maximum-entropy type deconvolution algorithm using the fact that the Odin beam is an almost circular Gaussian with sidelobes below −30 dB, paired with the strong ^{13}CO signal (see Hjalmarson et al. 2005).

From the column density map of Fig. 7 the total mass of H_2 gas in the mapped region is estimated to be 480 $M_\odot$, of which approximately 320 $M_\odot$ is situated in the direction of the molecular ridge. From the previous discussion we estimate that at least half of this mass belongs to the warm Orion PDR, while about half belongs to the bulk of the molecular ridge. This should be compared to the mass of very dense gas and condensations along the ridge, approximated to 200−300 $M_\odot$ from observations of CS and NH_3 (Batrla et al. 1983; Mundy et al. 1986; Mundy et al. 1988).

We have also convolved the column density map to 9′ resolution and estimated the beam-averaged H_2 column density to be 2×10^{22} cm^{-2}. This estimate is useful as an independent

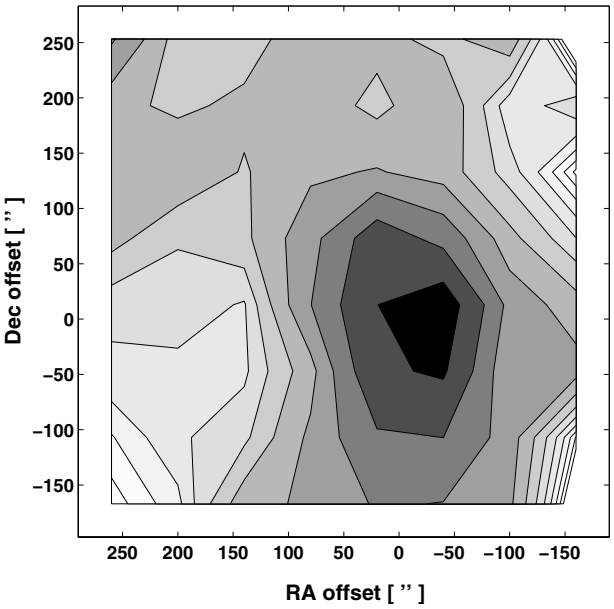

Fig. 7. Column density distribution of H_2 gas from the simple LTE model. At least half of the column in the direction of the molecular ridge belongs to the warm Orion PDR gas, see text. The ten contours are logarithmically spaced from $10^{21.7}$ cm^{-2} (white) to $10^{22.7}$ cm^{-2} (black). The two positions at the NW and SW corner of the map have been omitted.

reference for the deep O_2 searches with Odin at 119 GHz (cf. Pagani et al. 2003). Combined with the upper O_2 column density limit reached by Pagani et al. (2003) we get the abundance limit $O_2/H_2 \leq 9.5 \times 10^{-8}$, which is essentially the same as deduced by them.

In our previous analysis the kinetic temperature of the emitting gas was estimated from the measured CO peak main-beam temperature. However, the Rayleigh-Jeans approximation is not very good at the frequencies and temperatures of interest here, since $T_B > T_{RJ}$ by up to 35% (at 50 K). On the other hand, as noted above, no more than 40% of the ^{13}CO $J = 5-4$ emission comes from within the molecular ridge where the kinetic temperature is lower than in the Orion PDR, so this temperature is most likely an overestimate in turn. If the assumed T_{kin} is increased by 30% the column densities modelled with RADEX decrease by 10−25%, while a 30% lower input temperature gives larger column densities by 30−50% (largest effect at lowest temperatures).

4.4. Preliminary PDR ortho-water abundance estimates

Only in the Orion KL molecular cloud the *SWAS* and Odin satellites have observed uniquely strong and very extended narrow-line ortho-H_2O ($1_{10}-1_{01}$) emission (Snell et al. 2000; Olofsson et al. 2003). This emission is believed not to originate in the relatively cold dense cloud core (where the water presumably is mainly frozen out on grain surfaces), but instead must come from the heated Orion PDR – the region also traced by our current CO, and partly ^{13}CO and C^{18}O, $J = 5-4$, data. However, there is only indirect evidence supporting this scenario. As reported by Melnick & Bergin (2005) there is a striking correlation between the H_2O ($1_{10}-1_{01}$) integrated intensity mapped by *SWAS* across Orion KL and the corresponding CN $N = 1-0$ integrated intensity (where CN is a PDR, surface tracer), while there is no correlation at all with the observed C^{18}O $J = 1-0$ integrated intensity (a volume tracer).

In order to estimate the ortho-H_2O abundance relative to H_2 in the Orion PDR, for the three positions in Fig. 4, we adopt the method described by Snell et al. (2000). The method is based on the fact that, although the emission from the water transition in question becomes optically thick already at relatively small column densities, the high critical density (10^8 cm^{-3}), together with photon trapping, makes it "effectively optically thin" at the current densities (10^5 cm^{-3}). For the $1_{10}-1_{01}$ transition the ortho-H_2O abundance ratio can then be expressed as

$$x(\mathrm{o-H_2O}) = 6.0 \times 10^8 \, \frac{\int T_R \, dv}{C(T_K)\, N(H_2)\, n_{H_2}} \exp\,(26.8/T_K) \qquad (1)$$

where the collision coefficient (in cm^3 s^{-1}) depends on the kinetic temperature (T_K) in K, the integrated intensity is given in K km s^{-1}, the column density in cm^{-2}, and the density in cm^{-3}. As input we have first used the Odin H_2O data from Olofsson et al. (2003), presented in Fig. 4. The kinetic temperature, density and column density of the gas were then taken from our C^{18}O $J = 5-4$ analysis (see Table 3), but only using half of the resulting H_2 column density according to the PDR gas contribution estimate in Sect. 4.3. Using H_2 column density estimates obtained with the same telescope and beam-size as the water data, the errors due to beam filling are minimised. Finally, the collision coefficients for collisional excitation of ortho-H_2O by para- and ortho-H_2 were obtained from Phillips et al. (1996), at a temperature of 80 K in (0′, −2′) and 60 K in (+2′, −2′) and (+1′, +3′), assuming an LTE ratio of ortho- to para-H_2 of 1.07 (at 80 K). The average ortho-H_2O abundance ratios within the Odin beam in these positions, obtained through Eq. (1), are presented in Table 3.

The o-H_2O abundances presented in Table 3 are more than an order of magnitude higher than the typical ortho-H_2O abundance towards the Orion ridge, derived with the same method from *SWAS*-data, 5×10^{-9} (Snell et al. 2000). However, using a more elaborate statistical equilibrium code, these authors find about one order of magnitude larger abundances, $1-8 \times 10^{-8}$. The underestimate of Eq. (1) thus revealed is expected and mainly arises because of deviations from a simple two-level system. Since errors of the same magnitude should apply to our results, we find a significantly higher water abundance than that derived by Snell et al. (2000). We believe that this discrepancy mainly is a result of our effort to use an H_2 column that spatially better coincides with the origin of the observed water emission. Other factors influencing the result are the higher temperature assumed by us, decreasing the result through three times higher collision coefficient, and the one order of magnitude smaller density assumed by us. From a simple geometrical argument, the density assumed by us (10^5 cm^{-3}), in combination with the Orion PDR H_2 column densities used, leads to a PDR layer depth of the order of 10^{17} cm, in reasonable agreement with the Orion Bar thickness as observed e.g. in CO $J = 7-6$ by Wilson et al. (2001).

Another important feature of the energy level structure in H_2O is that the wavelengths of H_2O ($2_{21}-1_{10}$) and ($2_{12}-1_{01}$) lines are in the FIR ($\lambda \sim 110$ and ~ 180 μm). The strong and rather extended FIR radiation in the Orion KL region (e.g. Arimura et al. 2004) may thus alter the population distribution, yielding substantial errors also in the water abundances derived from statistical equilibrium codes. We believe that a proper modelling of this effect, preferrably including spatial variations

in the FIR field, is required to find more exact water abundances in the Orion KL region.

5. Conclusions

We have shown that by combining the temperature and column density information from the ^{12}CO and ^{13}CO $J = 5-4$ emission maps, we can derive the column density distribution of H_2 gas in the Orion KL region to a high level of certainty ($^{+50\%}_{-25\%}$). We find H_2 column densities ranging from 5×10^{21} cm^{-2} at map edges to 7×10^{22} cm^{-2} at the molecular ridge. We esimate that about half of this latter column density belongs to the warm Orion PDR. Based on data from three positions where C^{18}O $J = 5-4$ has been observed, we estimate the ortho-water abundance in the Orion PDR layer to be $\geq 8 \times 10^{-8}$, which is higher than previously estimated. Higher transitions in ^{13}CO or C^{18}O should trace the warm Orion PDR gas even better, so it would be desirable to obtain such maps, none of which has been published to date.

Our ultimate goal for this work is to apply a MEM-type deconvolution algorithm to CO, ^{13}CO, $J = 5-4$ and H_2O maps that very recently have been extended southwards to include the whole Orion Bar. This will make it possible to study H_2O abundance variations at an angular resolution comparable to that of Herschel Space Observatory at these wavelengths.

Acknowledgements. Generous financial support from the Research Councils and Space Agencies in Canada, Finland, France and Sweden is gratefully acknowledged. This research has made use of the on-line version of the statistical equilibrium radiative transfer code, RADEX, made available for public use as part of the Leiden Atomic and Molecular Database (LAMDA). Constructive comments from J. H. Black and the anonymous referee are greatly appreciated.

References

Arimura, S., et al. 2004, PASJ, 56, 51
Batrla, W., Wilson, T. L., Ruf, K., & Bastien, P. 1983, A&A, 128, 279
Bensch, F., Pak, I., Wouterloot, J. G. A., Klapper, G., & Winnewisser, G. 2001, ApJ, 562, L185
Bergin, E. A., Goldsmith, P. F., Snell, R. L., & Ungerechts, H. 1994, ApJ, 431, 674
Castets, A., Duvert, G., Dutrey, A. 1990, A&A, 234, 469
Frisk, U., Hagström, M., Ala-Laurinaho, J., et al. 2003, A&A, 402, L27
Fuente, A., Rodríguez-Franco, A., & Martín-Pintado, J. 1996, A&A, 312, 599
Genzel, R., & Stutzki, J. 1989, ARA&A, 27, 41
Genzel, R., Reid, M. J., Moran, J. M., & Downes, D. 1981, ApJ, 244, 884
González-Alfonso, E., Wright, C. M., Cernicharo, J., et al. 2002, A&A, 386, 1074
Graf, U. U., Genzel, R., Harris, A. I., et al. 1990, ApJ, 358, L49
Greaves, J. S., & Church, S. E. 1996, MNRAS, 283, 1179
Gustafsson, M., Kristensen, L. E., Clénet, Y., et al. 2003, A&A, 411, 437
Herrmann, F., Madden, S. C., Nikola, T., et al. 1997, ApJ, 481, 343
Hjalmarson, Å., Bergman, P., Biver, N., et al. 2005, Adv. Space Res., 36, 1031
Hollenbach, D. J., & Tielens, A. G. G. M. 1997, ARA&A, 35, 179
Howe, J. E., Jaffe, D. T., & Grossman, E. N. 1993, ApJ, 410, 179
Koepf, G. A., Fetterman, H. R., Clifton, B. J., et al. 1982, ApJ, 260, 584
Kristensen, L. E., Gustafsson, M., Field, D., et al. 2003, A&A, 412, 727
Lis, D. C., & Schilke, P. 2003, ApJ, 597, L145
Margulis, M., & Lada, C. J. 1985, ApJ, 299, 925
Marrone, D. P., Battat, J., Bensch, F., et al. 2004, ApJ, 612, 940
Masson, C. R., Lo, K. Y., Phillips, T. G., et al. 1987, ApJ, 319, 446
Melnick, G. J., & Bergin, E. A. 2005, Adv. Space Res., 36, 1027
Mundy, L. G., Scoville, N. Z., Baath, L. B., Masson, C. R., & Woody, D. P. 1986, ApJ, 304, L51
Mundy, L. G., Cornwell, T. J., Masson, C. R., et al. 1988, ApJ, 325, 382
Olberg, M., Frisk, U., Lecacheux, A., et al. 2003, A&A, 402, L35
Olofsson, A. O. H., Olofsson, G., Hjalmarson, Å., et al. 2003, A&A, 402, L47
Pagani, L., Olofsson, A. O. H., Bergman, P., et al. 2003, A&A, 402, L77
Pardo, J. R., Cernicharo, J., Herpin, F., et al. 2001, ApJ, 562, 799
Phillips, T. R., Maluendes, S., & Green, S. 1996, ApJS, 107, 467
Plambeck, R. L., Wright, M. C. H., & Rao, R. 2003, ApJ, 594, 911
Plume, R., Bensch, F., Howe, J. E., et al. 2000, ApJ, 539, L133
Rodríguez-Franco, A., Martín-Pintado, J., & Fuente, A. 1998, A&A, 329, 1097
Rodríguez-Franco, A., Wilson, T. L., Martín-Pintado, J., & Fuente, A. 2001, ApJ, 559, 985
Salas, L., Rosado, M., Cruz-González, I., et al. 1999, ApJ, 511, 822
Schilke, P., Benford, D. J., Hunter, T. R., Lis, D. C., & Phillips, T. G. 2001, ApJS, 132, 281
Schloerb, F. P., Irvine, W. M., Friberg, P., Hjalmarson, A., & Hoglund, B. 1983, ApJ, 264, 161
Schmid-Burgk, J., et al. 1989, A&A, 215, 150
Schöier, F. L., van der Tak, F. F. S., van Dishoeck, E. F., & Black, J. H. 2005, A&A, 432, 369
Schulz, A., Henkel, C., Beckmann, U., et al. 1995, A&A, 295, 183
Snell, R. L., et al. 2000, ApJ, 539, L93
Stacey, G. J., Jaffe, D. T., Geis, N., et al. 1993, ApJ, 404, 219
Ungerechts, H., Bergin, E. A., Goldsmith, P. F., et al. 1997, ApJ, 482, 245
Watson, D. M., Genzel, R., Townes, C. H., & Storey, J. W. V. 1985, ApJ, 298, 316
Werner, M. W., Gatley, I., Becklin, E. E., et al. 1976, ApJ, 204, 420
White, G. J., & Sandell, G. 1995, A&A, 299, 179
Wilson, T. L., & Matteucci, F. 1992, A&A Rev., 4, 1
Wilson, T. L., Mauersberger, R., Gensheimer, P. D., Muders, D., & Bieging, J. H. 1999, ApJ, 525, 343
Wilson, T. L., Muders, D., Kramer, C., & Henkel, C. 2001, ApJ, 557, 240
Wright, M. C. H., Plambeck, R. L., Mundy, L. G., & Looney, L. W. 1995, ApJ, 455, L185
Young Owl, R. C., Meixner, M. M., Wolfire, M., Tielens, A. G. G. M., & Tauber, J. 2000, ApJ, 540, 886
Yusef-Zadeh, F. 1990, ApJ, 361, L19
Zuckerman, B. 1973, ApJ, 183, 863
Zuckerman, B., Kuiper, T. B. H., & Rodriguez Kuiper, E. N. 1976, ApJ, 209, L137